land

MDPI

Article

Spatial and Seasonal Variation and the Driving Mechanism of the Thermal Effects of Urban Park Green Spaces in Zhengzhou, China

Yuan Feng [1], Kaihua Zhang [1], Ang Li [1], Yangyang Zhang [2], Kun Wang [1], Nan Guo [1], Ho Yi Wan [3], Xiaoyang Tan [4], Nalin Dong [1], Xin Xu [5], Ruizhen He [1], Bing Wang [6], Long Fan [7], Shidong Ge [1,*] and Peihao Song [1,*]

[1] College of Landscape Architecture and Art and International Union Laboratory of Landscape Architecture, Henan Agricultural University, Zhengzhou 450002, China; fy9987@outlook.com (Y.F.); kaihuazhang@stu.henau.edu.cn (K.Z.); leon@henau.edu.cn (A.L.); wkun@henau.edu.cn (K.W.); nuaunu@henau.edu.cn (N.G.); dongnalin@henau.edu.cn (N.D.); hrzzjd@henau.edu.cn (R.H.)
[2] Zhengzhou Green and Low-Carbon Building Design and Smart Construction Research, Zhengzhou 450002, China; zhangyangyang629@sina.com
[3] Department of Wildlife, California State Polytechnic University Humboldt, 1 Harpst Street, Arcata, CA 95521, USA; hw83@humboldt.edu
[4] Institute for Global Environmental Strategies (IGES), 2108-11 Kamiyamaguchi, Hayama, Kanagawa 240-0115, Japan; tan@iges.or.jp
[5] China Association of Building Energy Efficiency, Beijing 100089, China; xpku2010@163.com
[6] Henan Provincial Institute of Land and Space Investigation and Planning, Zhengzhou 450018, China; ct202409@163.com
[7] Henan Urban and Rural Planning and Design Research Institute Co., Ltd., Zhengzhou 450053, China; 117862031@163.com
* Correspondence: shidongge@henau.edu.cn (S.G.); peihaos@henau.edu.cn (P.S.)

Abstract: Greenscaping, a key sustainable practice, helps cities combat rising temperatures and climate change. Urban parks, a pivotal greenscaping element, mitigate the urban heat island (UHI) effect. In this study, we utilized high-resolution remote sensing imagery (GF-2 and Landsat 8, 9) and in situ measurements to analyze the seasonal thermal regulation of different park types in Zhengzhou, China. We calculated vegetation characteristic indices (VCIs) and landscape patterns (LMs) and employed boosted regression tree models to explore their relative contributions to land surface temperature (LST) across different seasons. Our findings revealed that urban parks lowered temperatures by 0.65 °C, 1.41 °C, and 2.84 °C in spring, summer, and autumn, respectively, but raised them by 1.92 °C in winter. Amusement parks, comprehensive parks, large parks, and water-themed parks had significantly lower LSTs. The VCI significantly influenced LST in autumn, with trees having a stronger cooling effect than shrubs. LMs showed a more prominent effect than VCIs on LST during spring, summer, and winter. Parks with longer perimeters, larger and more dispersed green patches, higher plant species richness, higher vegetation heights, and larger canopies were associated with more efficient thermal reduction in an urban setting. The novelty of this study lies in its detailed analysis of the seasonal thermal regulation effects of different types of urban parks, providing new insights for more effective urban greenspace planning and management. Our findings assist urban managers in mitigating the urban surface heat effect through more effective urban greenspace planning, vegetation community design, and maintenance, thereby enhancing cities' potential resilience to climate change.

Keywords: landscape metrics (LMs); land surface temperature (LST); urban ecology; urban parkland; vegetation characteristic index (VCI); urban heat island (UHI); boosted regression trees

Citation: Feng, Y.; Zhang, K.; Li, A.; Zhang, Y.; Wang, K.; Guo, N.; Wan, H.Y.; Tan, X.; Dong, N.; Xu, X.; et al. Spatial and Seasonal Variation and the Driving Mechanism of the Thermal Effects of Urban Park Green Spaces in Zhengzhou, China. *Land* **2024**, *13*, 1474. https://doi.org/10.3390/land13091474

Academic Editor: Guoyu Ren

Received: 18 July 2024
Revised: 7 September 2024
Accepted: 9 September 2024
Published: 11 September 2024

1. Introduction

According to United Nations projections, by 2050, urban areas will be home to 68% of the world's population [1]. Between 1990 and 2020, China's population grew by 24.4%,

with the urban population doubling and the rural population decreasing by 41.0%, indicating a significant trend towards urbanization [2]. Rapid urbanization poses various challenges to urban living spaces, including escalating concerns such as mental health issues, environmental pollution, overcrowding, and noise pollution [3–5]. The UHI effect, exemplifying the consequences of rapid urbanization on global climate change, is one of the significant concerns [6]. The UHI effect represents the deterioration of urban thermal conditions, leading to increased rates of heat-related illnesses and mortality among urban residents, thereby affecting public health [7,8]. Research conducted in Shanghai highlights a significant increase in heat-related mortality rates within urban areas compared to their surrounding regions during the summer season [9]. A study [10] revealed a clear positive correlation between maximum temperature and heat-related illnesses, noting that the heat impact is nonlinear and can persist for up to 3 days. Given the pressing need to mitigate the adverse effects of urban heat islands, this study aims to provide a more comprehensive understanding of the key factors influencing LST in urban parks and to develop recommendations for optimizing their cooling effects, thereby contributing valuable insights for more sustainable urban planning.

Greenscaping, a landscape design program that deliberately utilizes green infrastructure, is widely acknowledged as an effective passive method for reducing heat effects [11,12]. Urban park green spaces typically help mitigate the negative impact of impervious surfaces on urban surface temperatures, playing a crucial role in improving urban climate conditions [13,14]. Through shading and evapotranspiration by vegetation and water bodies, green spaces in urban parks help lower temperatures and increase humidity in the surrounding environment, serving as essential elements of the urban landscape. With advancing urbanization and growing societal emphasis on the ecological environment, the scarcity and importance of urban park green spaces have become more prominent. However, during the early stages of urbanization in many cities, the inevitable reduction in urban park areas occurs due to rapid population growth and the demand for residential space, resulting in a spatial mismatch between green space supply and demand.

Research on LST highlights the significant roles of both landscape patterns [15,16], which operate at a more macro level, and vegetation characteristic indices [17], which provide a more micro-level perspective, in mitigating the adverse effects of LST. A pronounced nonlinear correlation between UHI effects and landscape morphological indices has been observed in both intra-urban and extra-urban configurations [18]. Notably, the contribution of intra-urban morphological factors appears to be more substantial [19]. Ref. [20] discovered a connection between mortality rates and the density of urban structures during the severe heat waves of 1994 and 2006.

Research on surface heat effects in China started relatively late but has grown quickly since 2008. Previous research exhibits a clear geographical bias, primarily focusing on economically developed metropolises and select coastal cities. The impact of a city's geographical location [21] and climatic conditions [22,23] on UHI effects has been confirmed by numerous studies. Investigations into the seasonality of the thermal environment in urban park green spaces are confounded by influences from the geographical location and local hydrogeological settings, leading to mixed results across different studies. For example, Shenzhen, located in a subtropical marine monsoon climate zone, maintains an average summer temperature of 29.66 °C, with a fluctuation range of 40.99–21.15 °C [24]. In contrast, Hanoi, Vietnam, situated in a subtropical climate zone, experiences an average summer temperature of 40.38 °C [25]. However, there are certain commonalities and patterns in the spatial and temporal distribution of surface thermal environments across various regions [26,27]. In this study, we focus on Zhengzhou, a representative inland city with pronounced UHI effects, situated in a temperate continental monsoon climate. Zhengzhou's flat terrain and consistent climate minimize the influence of topographic [28,29] and climatic [30,31] variability on LST differences among parks. This reduction in external uncertainties enhances the reliability and generalizability of our findings.

While there are some studies investigating the impact of internal landscape variations within urban parks on LST, such as [32–34], the majority of research still tends to categorize parks as a single land use type, which may overlook the specific characteristics and variations within individual parks. Our study aims to fill this gap by investigating how different types of urban parks, with varied landscape structures and vegetation characteristics, influence LST, providing a more detailed understanding of these effects. Furthermore, we propose practical recommendations based on marginal effects analysis to optimize the cooling effects of different types of urban parks. This study offers insights that can help improve urban planning strategies to mitigate the UHI effect, thereby supporting sustainable development. By concentrating on these underexplored aspects, our research provides a theoretical basis for future ecological urban development and optimized park design.

2. Materials and Methods

2.1. Study Area

Zhengzhou City (E 112°42′–114°14′, N 34°16′–34°58′), with an area of 7567 km^2, is one of the 14 mega-cities in China and a representative city in the Central Plains region (Figure 1). According to Chinese population statistics, Zhengzhou's permanent population grew by 46% over the past 10 years, reaching 12.742 million. Zhengzhou resides within the warm temperate continental monsoon climate zone, boasting an average annual temperature of 14.7 °C and precipitation averaging 632.4 mm annually, with the majority falling during August. The urban terrain of Zhengzhou is predominantly flat, featuring a network of 124 rivers that flow through the two major river basins of the Yellow River and the Huai River (on the south side of the site). The vegetation is characteristic of the warm temperate deciduous broad-leaved forest type, with common plant species including *Populus tomentosa*, *Salix matsudana*, *Koelreuteria paniculata*, and *Acer negundo*. The soil in Zhengzhou primarily consists of warm temperate deciduous broad-leaved forest, dry forest, grassland, and brown soil, with the predominant soil types in the urban area being brown soil and tidal soil.

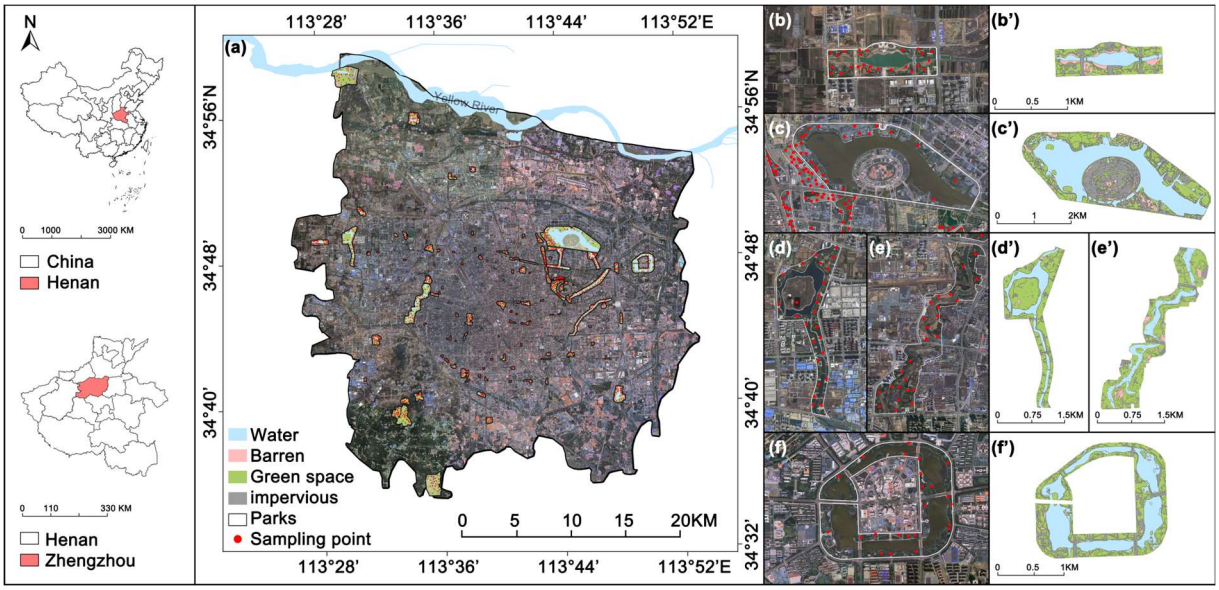

Figure 1. Location of Zhengzhou city, Henan, China. (**a**) Distribution of 123 selected parks in the study area versus 805 sampling points, (**b**–**f**) Distribution of sample sites in selected parks, (**b′**–**f′**) Selected parkland classification results.

2.2. Data and Methods

The experimental design of this study consists of four main stages (Figure 2). First, data acquisition was conducted using high-resolution (0.5 m) GF-2 remote sensing images,

30 m resolution Landsat 8 and 9 satellite imagery, and in situ measurements of vegetation characteristics within the parks. In the second stage, data processing was carried out, where the three datasets were utilized to calculate the LM, LST, and VCI for the 123 parks. The third stage involved classifying the 123 parks to observe the spatial heterogeneity in LST and the driving factors, including the LM and VCI. In the final stage, mathematical models and machine learning regression techniques were employed to identify the key driving factors for different parks across various seasons, and effective strategies were proposed to mitigate UHI effect for each park type.

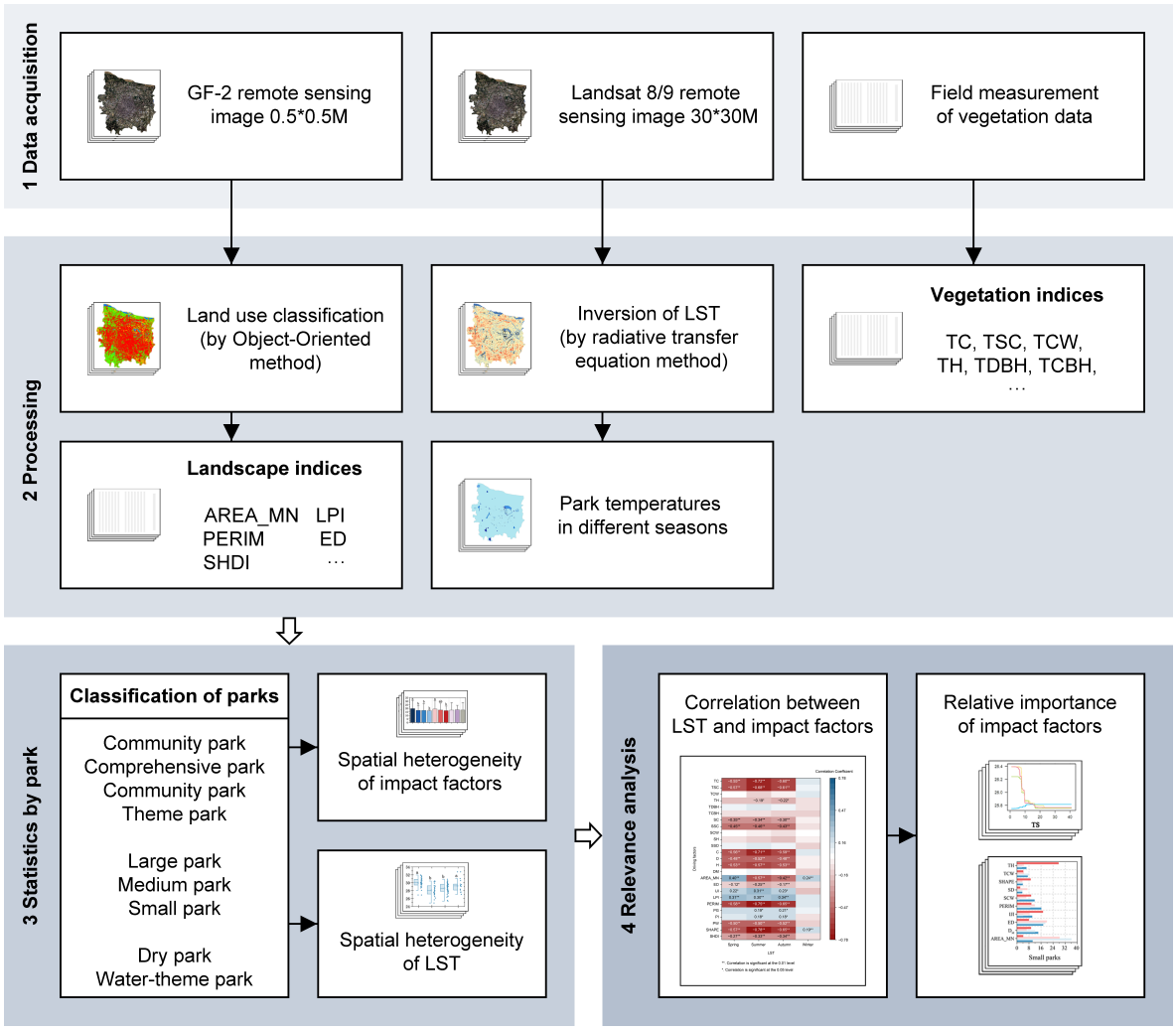

Figure 2. Flowchart of this study.

2.2.1. Parks Selection, Classification, and Field Survey

Based on criteria such as area, location, and level of development, 123 parks located in the central urban area were selected. Utilizing ArcGIS 10.5 and high-resolution GF-2 satellite imagery with a resolution of 0.5 m, combined with on-site observations, the vector boundaries of the 123 urban park green spaces were manually extracted (Figure 1).

The parks were categorized according to their size: small parks (<2 ha), medium-sized parks (2–10 ha), and large parks (>10 ha). Furthermore, following the guidelines outlined in the 'Classification Standard for Urban Green Spaces' (CJJ/T85-2017), which considers factors such as the ratio of paved areas, types of vegetation, and methods of vegetation maintenance, the parks were categorized into four distinct types: amusement parks, community parks, comprehensive parks, and theme parks. Water bodies are one of the most important landscape features affecting park LST and can provide significant

cooling effects. Therefore, the parks were further categorized into water-themed parks and dry parks based on the presence of water features.

The field sampling for this study was conducted from July to August 2021, encompassing a total of 123 parks. A total of 805 plots were randomly selected using ArcGIS Pro 3.0.2, with each sampling point centered in a 10-m radius circle for vegetation characteristics surveys. For parks smaller than 2.5 hectares, only one plot was selected. For parks larger than 2.5 hectares, an additional plot was selected for every additional 2.5 hectares. For example, a park reaching 5 hectares had two plots, and a park reaching 7.5 hectares had three plots, and so on, with a maximum of 25 plots per park. To ensure the accuracy of the results, each plot was required to be at least 100 m apart from adjacent plots.

To minimize the impact of internal variability on the experimental results, the average VCI from multiple plots within a single park was used to represent the entire park. This approach helps to reduce the influence of internal differences on the outcomes. When adjusting the sample point locations according to real-world conditions, high-resolution satellite images from Google Earth were utilized for accuracy. The adjusted sample point locations were recorded and cross-referenced with their latitude and longitude coordinates. Field surveys were then conducted at these confirmed locations.

2.2.2. Inversion of LST

The study initially divided the year into four seasons using the solar term method combined with local temperature data in Zhengzhou. March to May, June to August, September to November, and December to February were categorized as spring, summer, autumn, and winter, correspondingly. In this study, it was recognized that using single-time-point data to infer LST is influenced by numerous factors and is subject to significant randomness, making it unable to represent the LST characteristics over a specific period. Therefore, multiple sets of remote sensing imagery from 2019 to 2022 were selected, retaining 28 periods (Table 1) with an overall cloud cover of less than 1%, for LST inversion.

Table 1. Remote sensing data description.

Satellite	Sensor	Date	Satellite	Sensor	Date
Landsat 8	OLI_TIRS	12 November 2019	Landsat 8	OLI_TIRS	30 September 2021
Landsat 8	OLI_TIRS	31 January 2020	Landsat 8	OLI_TIRS	3 December 2021
Landsat 8	OLI_TIRS	16 February 2020	Landsat 8	OLI_TIRS	19 December 2021
Landsat 8	OLI_TIRS	19 March 2020	Landsat 9	OLI-2_TIRS-2	27 December 2021
Landsat 8	OLI_TIRS	4 April 2020	Landsat 9	OLI-2_TIRS-2	2 April 2022
Landsat 8	OLI_TIRS	22 May 2020	Landsat 8	OLI_TIRS	10 April 2022
Landsat 8	OLI_TIRS	26 August 2020	Landsat 9	OLI-2_TIRS-2	18 April 2022
Landsat 8	OLI_TIRS	11 September 2020	Landsat 9	OLI-2_TIRS-2	4 May 2022
Landsat 8	OLI_TIRS	29 October 2020	Landsat 9	OLI-2_TIRS-2	20 May 2022
Landsat 8	OLI_TIRS	16 December 2020	Landsat 9	OLI-2_TIRS-2	5 June 2022
Landsat 8	OLI_TIRS	1 January 2021	Landsat 8	OLI_TIRS	13 June 2022
Landsat 8	OLI_TIRS	17 January 2021	Landsat 8	OLI_TIRS	29 June 2022
Landsat 8	OLI_TIRS	2 February 2021	Landsat 9	OLI-2_TIRS-2	7 July 2022
Landsat 8	OLI_TIRS	22 March 2021	Landsat 8	OLI_TIRS	1 September 2022

The radiative transfer equation method is employed to estimate the atmospheric thermal impact on LST by utilizing standard atmospheric profile data. Subsequently, this component of thermal influence is subtracted from the total thermal radiation detected by the thermal infrared sensor. This method enables a more accurate depiction of land surface thermal radiation characteristics, yielding LST estimates with a precision of up to 0.6 °C [35]:

$$L_\lambda = [\varepsilon \, B(T_s) + (1 - \varepsilon) \, L\downarrow]\tau + L\uparrow \quad (1)$$

In Equation (1), L_λ represents the thermal infrared radiance received by the satellite sensor, ε denotes the land surface emissivity, $B(T_s)$ represents the blackbody radiance

($W \cdot m^{-2} \cdot sr^{-1} \cdot \mu m^{-1}$) corresponding to the land surface temperature (T_s). τ represents the atmospheric transmittance in the thermal infrared wavelength range, while $L\uparrow$ denotes the upwelling radiance from the atmosphere, and $L\downarrow$ represents the downwelling radiance reflected from the ground and reaching the sensor. ε is determined as below:

$$\varepsilon = 0.004P_v + 0.986 \quad (2)$$

$$P_v = \left(NDVI - NDVI_{soil} \Big/ NDVI_{veg} - NDVI_{soil} \right) \quad (3)$$

In Equation (3), $NDVI_{soil}$ and $NDVI_{veg}$ represent the values of NDVI when the land surface consists of bare soil (P_v = 0) and when vegetation cover is 100%, respectively [36]. After calculating the surface emissivity, the actual LST can be computed using the inverse function of the Planck equation, as shown in the following formula:

$$T_S = {K_2} \Big/ \ln\left[\frac{K_1}{B(T_S)} + 1 \right] \quad (4)$$

where T_S represents the actual LST in Kelvin (K). K_1 = 774.8853 $W \cdot m^{-2} \cdot sr^{-1} \cdot \mu m^{-1}$ and K_2 = 1321.0789 $W \cdot m^{-2} \cdot sr^{-1} \cdot \mu m^{-1}$, which are pre-defined constants before satellite emission.

2.2.3. Impact Factors

Based on the findings of field research, 15 VCIs were selected as explanatory variables for LST, comprising 6 indices associated with trees, 5 indices linked to shrubs, and 3 indices correlated with biodiversity (Table 2).

Table 2. Surface thermal environmental drivers and abbreviations.

Variable	Abbr.	Units	Description	Formula
Tree Count	TC	individuals	Total number of trees in sample plots	$TC = \sum_{i=1}^{TSC} n_i$
Tree Species Count	TSC	individuals	Total number of tree species in sample plots	-
Average Tree Crown Width	TCW	m	Mean width of tree crowns	$TCW = \frac{\sum_{i=1}^{TC} TCW_i}{TC}$
Average Tree Height	TH	m	Mean height of trees in sample plots	$TH = \frac{\sum_{i=1}^{TC} TH_i}{TC}$
Average Tree Diameter at Breast Height	TDBH	cm	Average diameter of tree trunks at 1.3 m above ground	$TDBH = \frac{\sum_{i=1}^{TC} TDBH_i}{TC}$
Tree Crown Base Height	TCBH	m	Mean height from ground to lowest branch of crown	$TCBH = \frac{\sum_{i=1}^{TC} TCBH_i}{TC}$
Shrub Count	SC	individuals	Total number of shrubs in sample plots	$SC = \sum_{i=1}^{SSC} n_i$
Shrub Species Count	SSC	individuals	Total number of shrub species in sample plots	-
Average Shrub Canopy Width	SCW	m	Mean width of shrub canopies	$SCW = \frac{\sum_{i=1}^{SC} SCW_i}{SC}$
Average Shrub Height	SH	m	Mean height of shrubs in sample plots	$SH = \frac{\sum_{i=1}^{SC} SH_i}{SC}$
Average Shrub Stem Diameter	SSD	cm	Average diameter of shrub stems	$SSD = \frac{\sum_{i=1}^{SC} SSD_i}{SC}$

Table 2. *Cont.*

Variable	Abbr.	Units	Description	Formula
Individual Count	C	individuals	Total number of individuals in sample plots	$C = TC + SC$
Simpson Index	D	-	Probability that two randomly selected individuals belong to the same species	$D = 1 - \sum_{i=1}^{N} (\frac{n_i}{C})^2$
Shannon-Wiener Index	H	-	Index accounting for species abundance and evenness	$H = -\sum_{i=1}^{N} (P_i \times \ln(P_i))$
Menhinick Index	D_M	-	Measure of species richness considering the number of species and individuals	$D_M = \frac{N}{\sqrt{C}}$
Mean Patch Size	AREA_MN	ha	Average size of landscape patches	$AREA\_MN = \frac{\sum_{i=1}^{patch\ count} patch\ area_i}{patch\ count}$
Edge Density	ED	m/ha	Total edge length in the landscape per unit area (per hectare)	$ED = \frac{total\ edge\ length}{total\ landscape\ area}$
Interspersion and Juxtaposition Index	IJI	%	Dispersion and juxtaposition of patch types (0: low, 100: high)	$IJI = \frac{actual\ adjacencies}{\max\ adjacencies} \times 100$
Largest Patch Index	LPI	%	Percentage of landscape occupied by the largest patch	$LPI = \frac{largest\ patch\ area}{total\ landscape\ area} \times 100$
Patch Perimeter	PERIM	m	Total boundary length of patches	-
Vegetation Cover Percentage	PG	%	Percentage of landscape covered by vegetation	$PG = \frac{vegetation\ area}{total\ landscape\ area} \times 100$
Impervious Surface Percentage	PI	%	Percentage of landscape covered by impervious surfaces	$PI = \frac{impervious\ area}{total\ landscape\ area} \times 100$
Water Body Percentage	PW	%	Percentage of landscape covered by water bodies	$PW = \frac{water\ body\ area}{total\ landscape\ area} \times 100$
Shape Index	SHAPE	-	Complexity of patch shapes relative to a standard shape (e.g., square)	$SHAPE = \frac{patch\ perimeter}{\sqrt{patch\ area_i}}$
Shannon Diversity Index	SHDI	-	Index considering species richness and evenness across patches	$SHDI = -\sum_{i=1}^{N} (P_i \times \ln(P_i))$

N represents the total number of species (both tree and shrub species) in the sample plots. n_i represents the number of individuals of the ith species. P_i represents the proportion of the ith species, calculated as $P_i = n_i/C$. TCW_i represents the crown width of the ith tree. TH_i represents the height of the ith tree. $TDBH_i$ represents the diameter at breast height of the ith tree. $TCBH_i$ represents the crown base height of the ith tree. SCW_i represents the canopy width of the ith shrub. SH_i represents the height of the ith shrub. SSD_i represents the stem diameter of the ith shrub. *patch count* represents the total number of patches in the landscape. $patch\ area_i$ represents the area of the ith patch in the landscape. $patch\ perimeter_i$ represents the perimeter of the ith patch in the landscape. *total landscape area* represents the total area of the landscape being studied. *actual adjacencies* represents the actual number of adjacent patch pairs. max *adjacencies* represents the maximum possible number of adjacent patch pairs.

Simultaneously, 10 dependent landscape indices, capable of comprehensively describing landscape patterns, were utilized as explanatory variables for LST. Firstly, land cover classification of the study area was conducted using high-resolution imagery from the GF-2 satellite. The background imagery was acquired on 25 May 2017, and 16 April 2018, with a spatial resolution of 1 m × 1 m. Following preprocessing of the GF-2 remote sensing images, an object-oriented approach was employed for map segmentation and classification. Classification accuracy was assessed using a confusion matrix, yielding an overall accuracy of 89.12% (refer to Figure 1b′–f′). Subsequently, the obtained results were inputted into Fragstats 4.2 software for analysis of landscape pattern features, resulting in the derivation of ten landscape indices.

2.2.4. Correlation between LST and Driving Factors

Urban park LST, under different seasons and types, is treated as the dependent variable, while the VCI and LM are considered independent variables to investigate the main driving factors in urban parks. After classifying the urban parks in Zhengzhou and calculating LST and influencing factors, one-way analysis of variance ($p < 0.05$) and independent samples T-tests are used to validate significant differences in LST means and driving factors among different types of parks during different seasons. Subsequently, a three-step process is employed to study the impact of driving factors on the LST of urban parks:

First, data samples are examined using the 1.5 times the interquartile range method to detect and discard outliers. Spearman correlation analysis ($p < 0.05$) is then employed to examine the significant relationships between driving factors and LST across seasons and park types. Second, boosted regression tree models are constructed in R 4.2.2 to explore the relative contributions of driving factors on seasonal LST and its variation. Bootstrap aggregating (bagging) fractions of 0.5 and 0.75 are used [27,37,38], and the optimal parameter solution is obtained through iterations during tree model construction. The final output model is validated through 10-fold cross-validation to investigate the impact of various driving factors on LST across different seasons and park types. Third, marginal effects illustrate how a single independent variable influences the prediction outcome while holding other variables constant. In this study, partial dependence plots are used to identify key variables affecting LST in different types of parks and to analyze their specific impacts on LST. This approach explores the reasonable range of changes in driving factors aimed at reducing surface temperature, providing a basis for decision-making in urban park green space planning.

3. Results

3.1. Characteristics of Spatial and Temporal Variability of LST in Parks

During autumn, parks exhibit a greater temperature difference compared to urban areas, with an average LST of 26.10 °C, which is 2.84 °C lower than that of the urban area (Figure 3, Table 3). However, in winter, the LST shows a slight elevation within parks compared to urban areas. During summer, the LST within parks varies between 31.32 °C and 40.67 °C, averaging at 37.30 °C. Hotspots within park areas are predominantly situated in the central urban region, showing a pattern of elevated LSTs towards the east and west, and relatively cooler LSTs towards the north and south. In spring, park LSTs show a minor elevation compared to autumn, averaging at 28.90 °C. Overall, park LSTs during this season are 0.65 °C lower than the urban average.

Table 3. LST in four seasons in parks of the study area.

Season	LST (°C)	Amusement Parks	Community Parks	Comprehensive Parks	Theme Parks	Small Parks	Medium-Sized Parks	Large Parks	Dry Parks	Water-Themed Parks
Spring	Maximum	8.75	30.43	30.89	32.75	31.95	32.75	31.05	32.75	30.55
	Minimum	26.9	24.87	25.34	27.07	27.92	24.87	25.34	24.87	25.34
	Average	29.99	28.09	28.6	29.23	30.06	28.91	28.16	29.45	27.93
	Standard Deviation	1.11	1.44	1.25	1.57	0.96	1.41	1.31	1.31	1.22
Summer	Maximum	40.67	37.9	38.7	39.76	40.67	39.76	37.37	40.67	37.81
	Minimum	35.35	32.74	31.32	33.92	34.95	32.74	31.32	32.23	31.32
	Average	37.73	35.26	35.1	36.01	37.83	36.06	34.52	36.62	34.59
	Standard Deviation	1.37	1.5	1.73	1.61	1.31	1.4	1.43	1.75	1.44
Autumn	Maximum	28.65	27.45	27.6	28.49	28.65	28.49	27.15	28.65	27.31
	Minimum	24.12	24.29	23.79	24.71	25.58	24.12	23.79	24.12	23.79
	Average	26.93	25.75	25.77	26.18	27	26.18	25.46	26.51	25.37
	Standard Deviation	0.97	0.87	0.91	1.01	0.82	0.93	0.8	0.96	0.74

Table 3. *Cont.*

Season	LST (°C)	Amusement Parks	Community Parks	Comprehensive Parks	Theme Parks	Small Parks	Medium-Sized Parks	Large Parks	Dry Parks	Water-Themed Parks
Winter	Maximum	7.86	8.42	8.75	8.14	7.84	8.06	8.75	8.75	8.37
	Minimum	3.99	5.56	5.23	5.74	4.74	3.99	5.23	3.99	4.9
	Average	6.5	6.82	6.86	7.09	6.58	6.68	7	6.84	6.69
	Standard Deviation	0.93	0.77	0.77	0.82	0.79	0.87	0.78	0.89	0.68

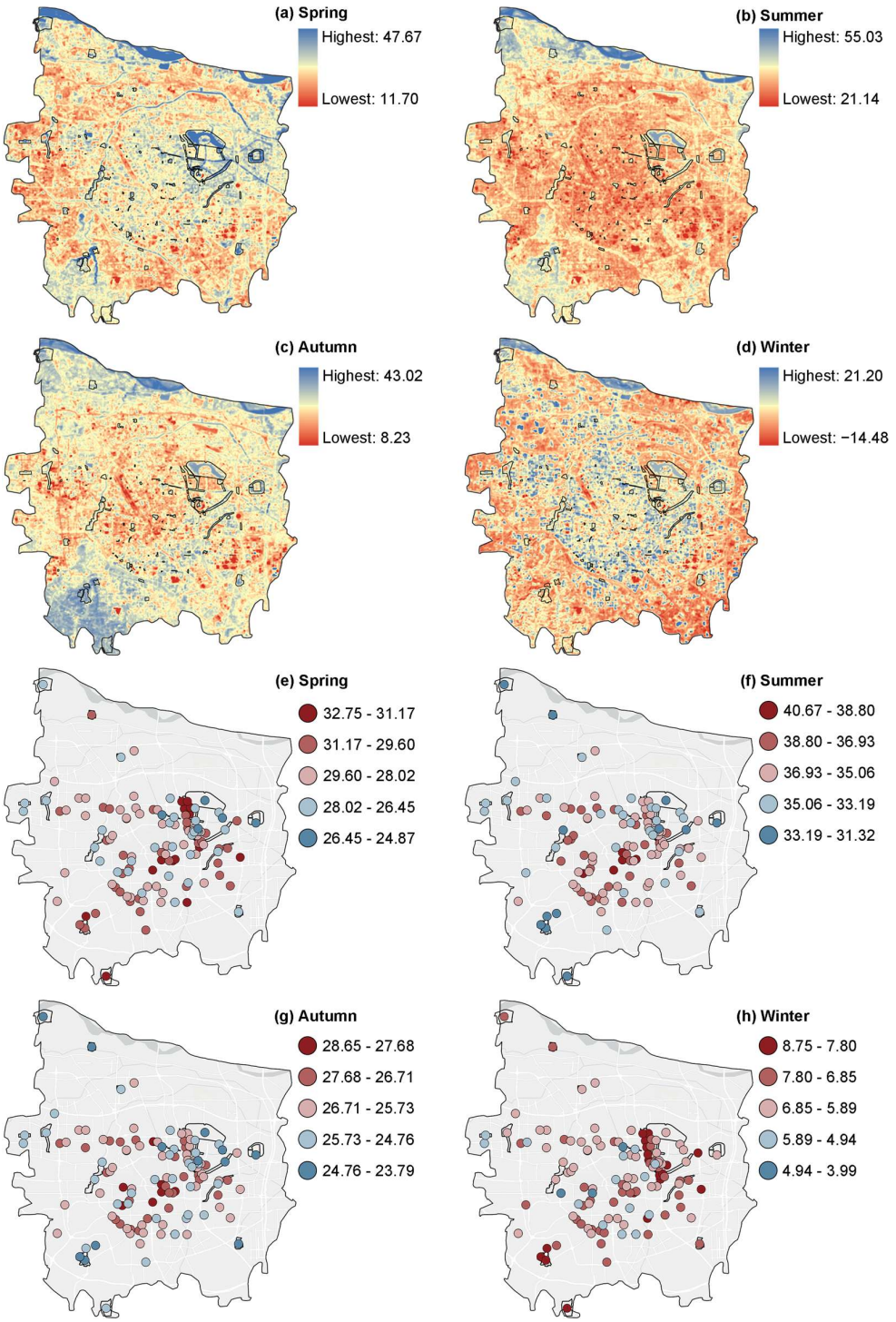

Figure 3. (**a**–**d**) LST in different seasons (Units: °C); (**e**–**h**) Land surface temperature of parks in different seasons.

The research also highlights substantial disparities in LST among various park types during spring, summer, and autumn, though these distinctions are less pronounced during winter. Except for winter, large parks and water parks exhibit lower LSTs, while amusement parks, small parks, and dry parks have higher average temperatures compared to other parks (Figure 4). In contrast, during winter, the distribution of LSTs among different types of parks is completely reversed, with theme parks, large parks, and water-themed parks having higher LSTs. During spring, amusement parks and theme parks have higher LSTs, averaging 29.99 °C and 29.23 °C, respectively. In summer and autumn, the average LST of amusement parks is 37.73 °C and 26.91 °C, respectively. Throughout spring, summer, and autumn, there is a notable decline in LST as park area increases, and dry parks exhibit significantly higher LST than water-themed parks. In winter, the LST of small parks (6.58 °C) is lower than that of large parks (7.0 °C). These findings indicate that there are statistically significant differences in LST among different types of parks during different seasons, and various classification indicators have a significant influence on the LST of parks during different seasons. These findings show statistically significant differences in LST among park types across seasons, with various classification indicators strongly influencing park LST during different seasons.

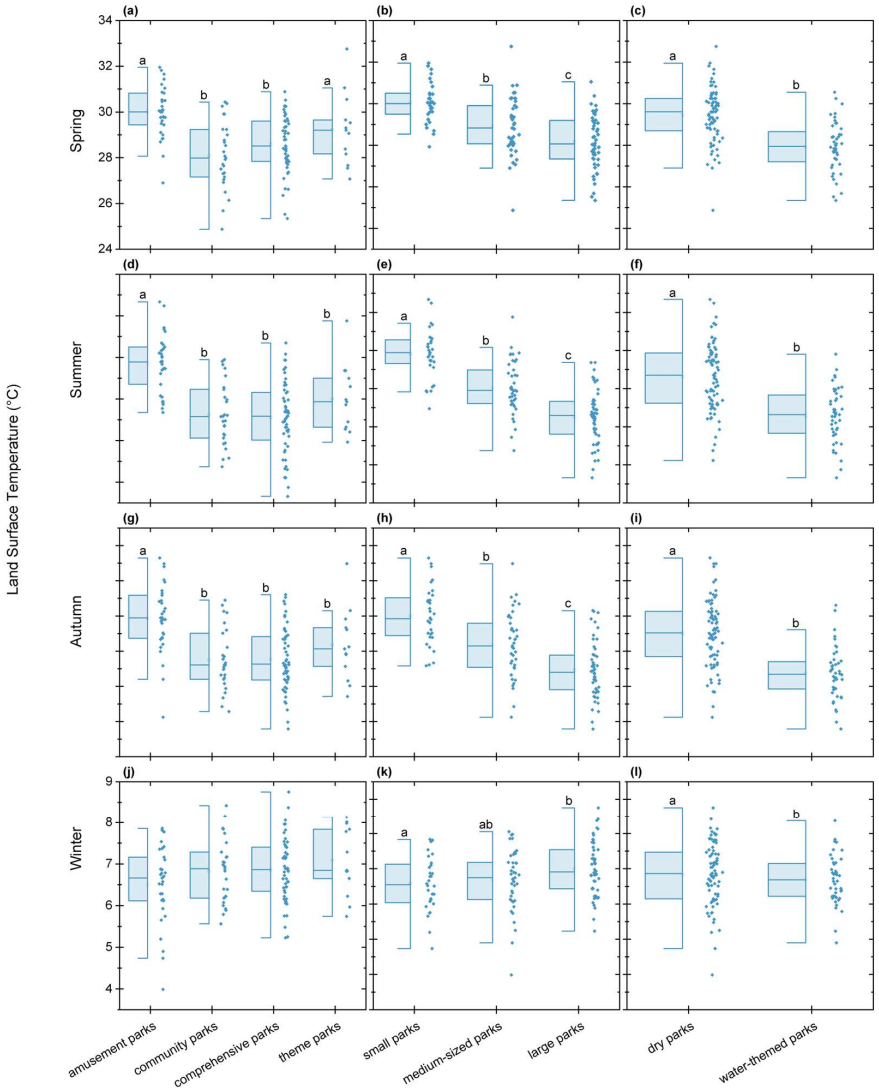

Figure 4. Differences in LST categories among parks in different seasons. The letters a, b, and c denote significant disparities identified via Fisher's least significant difference test ($p < 0.05$) across various park types during different seasons. (**a**–**c**), (**d**–**f**), (**g**–**i**), and (**j**–**l**) represent the LST distribution of parks classified by different standards in spring, summer, autumn, and winter, respectively.

3.2. Spatial Changes in Impact Factors

For the VCI, among various park types, amusement parks have notably smaller TSC, TC, S, and H values compared to others, while their TDBH value significantly exceed that of others, reaching 19.52 cm (Figure 5). Theme parks have significantly higher TH compared to other parks, with a value of 5.77 m. When comparing parks of different sizes, the values of H, TSC, and TC decrease gradually as the park area decreases, while D shows the opposite trend. Large parks exhibit significantly higher SSC compared to other parks, with an average of 18 species. Additionally, SC, DM, and S in large parks are significantly larger than in small parks, while TDBH is significantly smaller than in small parks. This indicates that large parks have a greater variety of plant species, and the distribution of species is more even. In water-themed parks compared to dry parks, water-themed parks have significantly higher values for TH, TSC, TC, TCBH, SSC, SC, DM, S, and H, while SSD and D values are significantly lower in water-themed parks, measuring 11.73 cm and 0.13, respectively. This suggests that water-themed parks generally have better conditions for tree species in terms of various indicators, including species richness, quantity, and overall status. Water-themed parks also tend to have higher numbers of species, greater species richness, and more even distribution. Overall, the distribution of vegetation indices varies among different parks, and comprehensive parks, large parks, and water-themed parks demonstrate clear advantages in terms of species diversity, richness, and evenness.

For the LM, there is a relatively small variation in landscape fragmentation among different park types, while significant differences exist in patch diversity and land cover types (Figure 5). PI and AREA_MN show weak differences among parks, whereas other landscape indices exhibit significant variations among different park types. Among parks with different characteristics, the LPI of amusement parks is significantly higher compared to other parks, while PERIM and SHDI show the opposite trend. In parks with different sizes, PERIM increases with park area, and large parks have significantly higher SHDI and lower ED. Small parks have significantly higher PG and LPI compared to large parks, while PW and IJI show the opposite pattern. In water-themed parks and dry parks, PW, IJI, PERIM, SHAPE, and SHDI are significantly higher in water-themed parks, while LPI and PG show the opposite trend.

3.3. Corrections between LST and Impact Factors

To examine their correlation with LST in different seasons, all 25 factors were included in the correlation analysis. Figure 6 displays the varying degrees of correlation between LST and influencing factors across different seasons. Overall, the correlations between the indicators and LST are stronger in spring, summer, and autumn compared to winter. (Figure A1 illustrates the results of the correlation analysis between LST and influencing factors for different types of parks under different seasons). From spring to autumn, significant negative correlations were observed between LST and TC, TSC, SC, SSC, C, D, H, PERIM, PW, SHAPE and SHDI. Notably, during summer, C, PERIM and SHAPE exhibited the strongest correlations of -0.71, $-0,75$ and -0.78, respectively. Conversely, IJI and LPI showed significant positive correlations with LST. Among them, PERIM and SHAPE had the strongest correlation in autumn (both -0.65), while PERIM had the strongest correlation in spring (-0.58), and AREA_MN had the strongest correlations in winter (0.24).

3.4. Relative Importance of Impact Factors

To address model overfitting, 5 VCI and 5 LM variables that have a significant impact on LST were selected. These variables were incorporated into an enhanced regression tree model for model construction, enabling us to further analyze their relative contributions to LST under complex conditions. The results revealed that the VCI had a higher contribution rate to LST during autumn, accounting for 50.33%, while the LM exhibited the highest contribution rate in winter, with a value of 61.65% (see Figure 7).

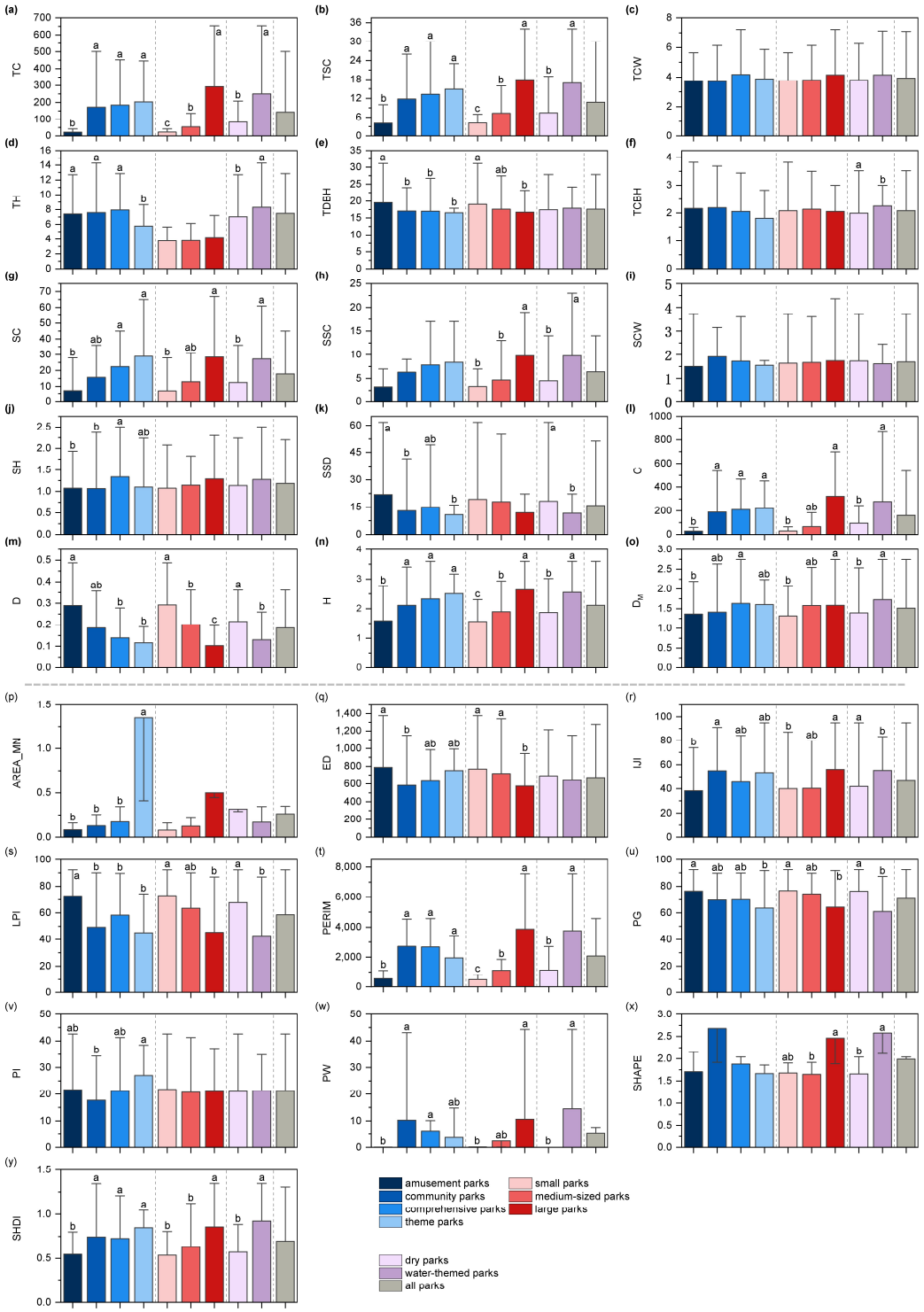

Figure 5. Analysis of the differences in driving factors among different park types. The letters a, b, and c denote significant disparities identified via Fisher's least significant difference test ($p < 0.05$) among different park types. (**a**–**o**) are vegetation characteristic indices, and (**p**–**y**) are landscape pattern indices.

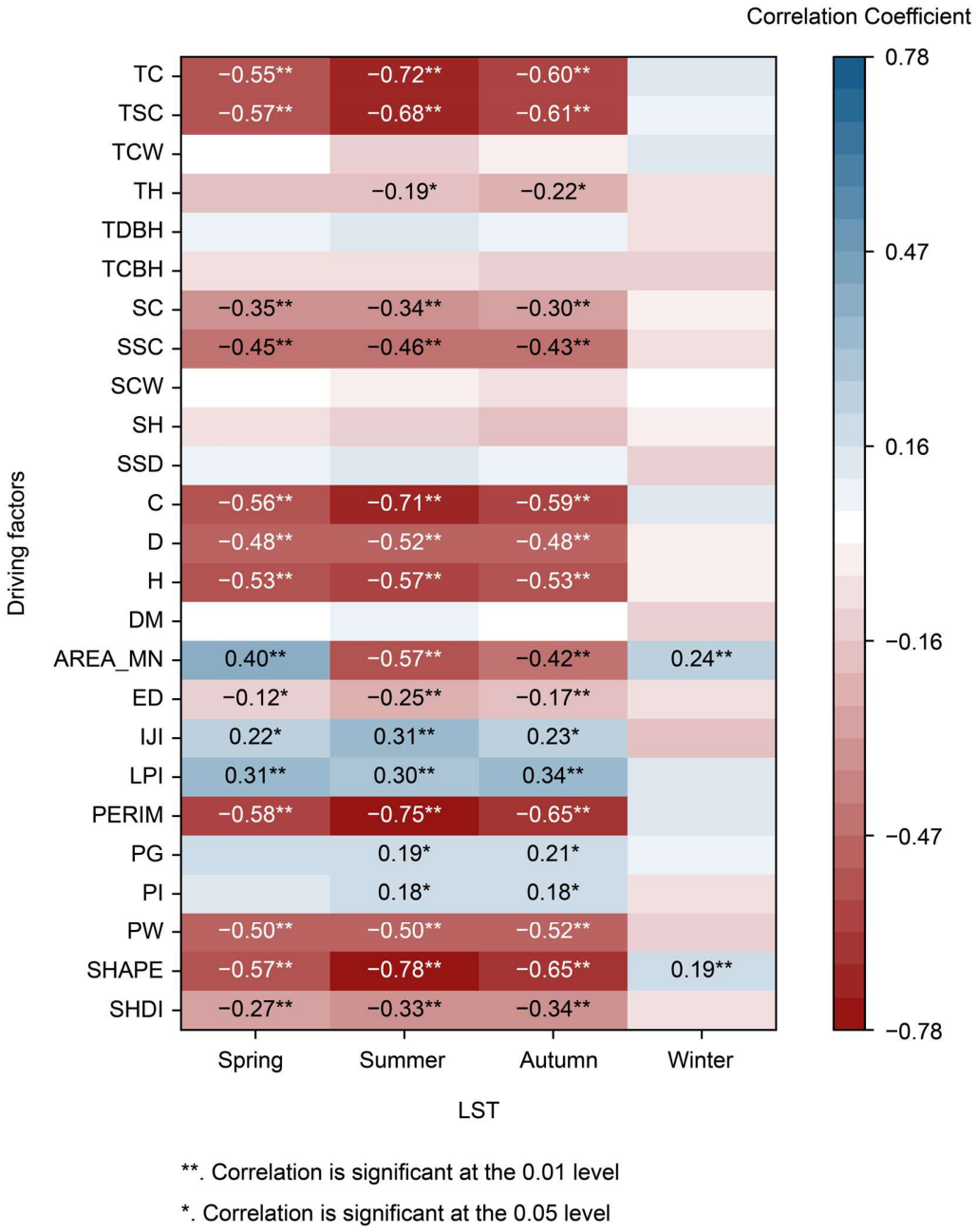

Figure 6. Spearman correlation coefficients of influencing factors with LST across seasons. (**. Correlation is significant at the 0.01 level; *. Correlation is significant at the 0.05 level).

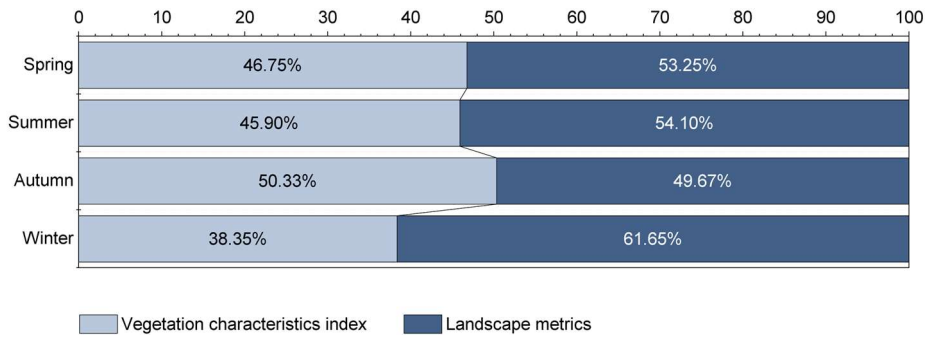

Figure 7. Relative contribution of each influencing factor to surface temperature under different seasons.

Based on the classification of park types, except for theme parks during winter, the contribution of the LM is higher than that of the VCI (Figure 8). In amusement parks, TCW, PERIM, and AREA_MN are the top three factors influencing LST in spring, summer, and autumn, accounting for a combined average contribution of 59.14% to LST variations. In winter, the dominant factor was SHAPE_MN, contributing 28.01%. In community parks, PERIM is the predominant driver of LST variations, contributing 39.32%, 38.06%, and 34.75% in summer, autumn, and spring, respectively, while AREA_MN becomes the major contributor during winter, with a contribution rate of 51.33%. In comprehensive parks, PERIM has the highest explanatory power for LST in spring, summer, and autumn, accounting for 39.24%, 39.24%, and 37.84%, respectively, while SHAPE becomes the primary factor in winter, contributing 20.04%. In theme parks, AREA_MN, ED, and SHAPE have significant effects on LST from spring to autumn, contributing to a total contribution rate of 75.58%, 88.2%, and 71.84%, respectively, across different seasons.

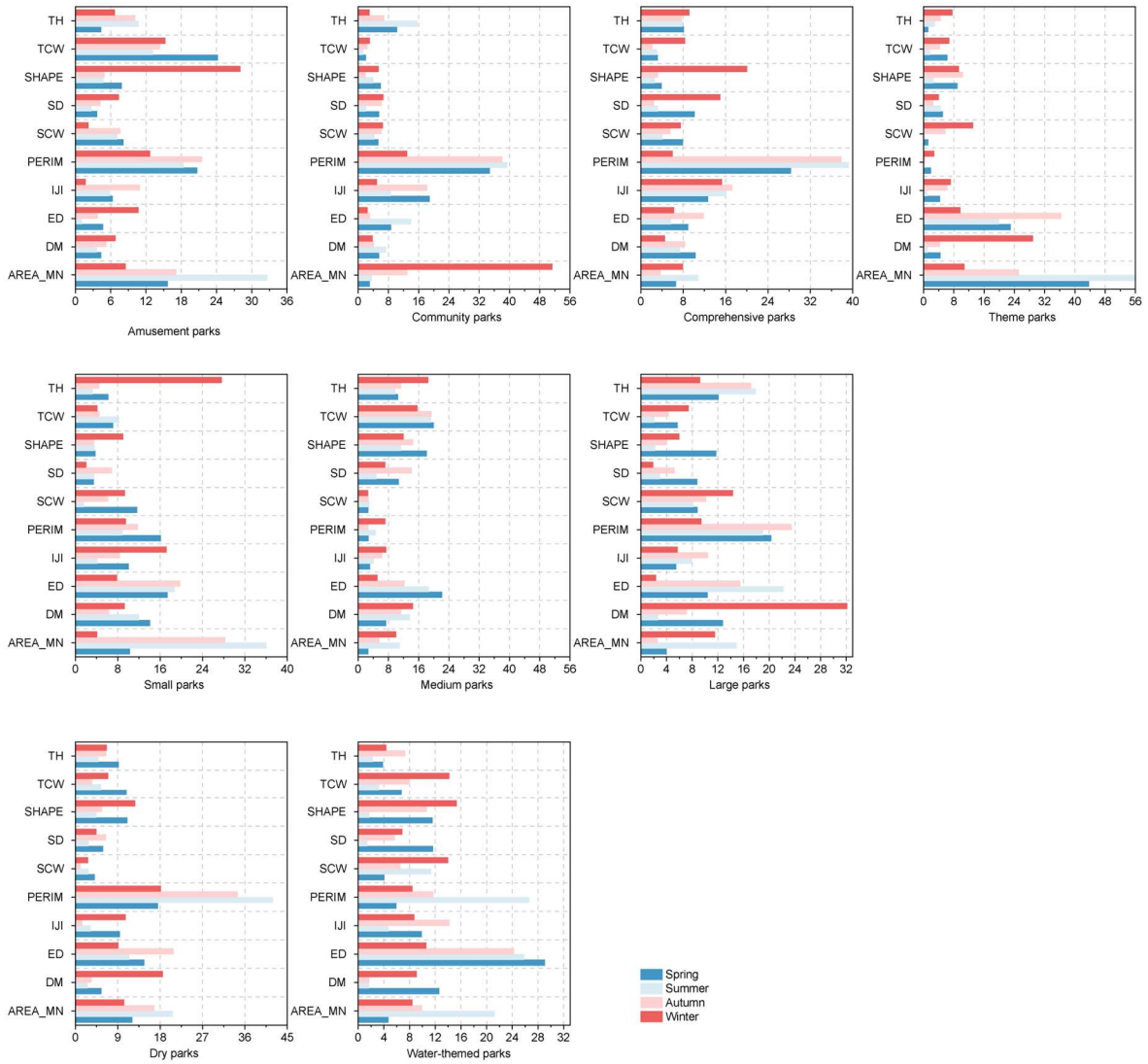

Figure 8. Relative importance of different park types for surface temperature in different seasons (%).

In terms of park size, in small parks, the factors contributing the most to LST in winter are TH (27.59%) and IJI (17.2%), while in other seasons, the major factors are PERIM, AREA_MN, ED, and DM (Figure 8). In medium parks, the significant contributors to LST variation are TCW, DM, SHAPE, and ED, with the average total contributions to park LST ranking as follows: spring (67.59%) > summer (62.83%) > autumn (57.33%) >

winter (47.18%). In large parks, PERIM has the highest contribution in spring and autumn, followed by TH, while in summer, ED explains 22.20% of the variation, followed by PERIM at 19.01%. In winter, DM has the highest contribution (32.15%).

Comparing parks with and without water bodies, the LM has a stronger relative contribution to LST in dry parks, while in water-themed parks, the total contribution of the LM to LST is higher in summer compared to the VCI, but the opposite is observed in other seasons (Figure 8). In water-themed parks, the significant factors contributing to LST in spring, summer, and autumn are PERIM, AREA_MN, and ED, with the total contributions ranking as summer (73.95%) > autumn (92%) > spring (44.21%). In winter, the major contributors to LST in parks without water are DM, PERIM, and SHAPE, with contributions of 18.51%, 18.09%, and 12.66%, respectively.

3.5. Marginal Effects

Most VCIs show consistent cooling effects on LST during spring, summer, and autumn, with a stronger impact observed during summer and autumn (Figure 9). TCW has a positive contribution to park LST throughout the year, with the contribution magnitude ranking as autumn > spring > summer > winter. SSD shows a slightly decreasing and then increasing trend in its contribution to LST in spring, summer, and autumn, with the strongest influence observed in summer and a decreasing trend during winter, with a controlled magnitude of 0.2 °C. D_M and H exhibit fluctuating contributions to LST, with a downward trend, but the magnitude of fluctuations shows distinct seasonal differences. Except for winter, TSC and TC have negative impacts on park LST, with stronger control magnitudes during summer and autumn, at 0.75 °C and 1.6 °C, respectively. SSC shows a rising and then a stepwise decline trend in its contribution to LST across the four seasons, with inflection points at 2.5, 5, 3.7, and 3. On the other hand, SH, SC, and D exhibit varying contributions to park LST across different seasons, without clear changing trends. These results demonstrate that by controlling the value of the VCI, within a certain range, beneficial effects on the surface thermal environment can be achieved. Therefore, vegetation planting and maintenance can be utilized to regulate LST to a certain extent.

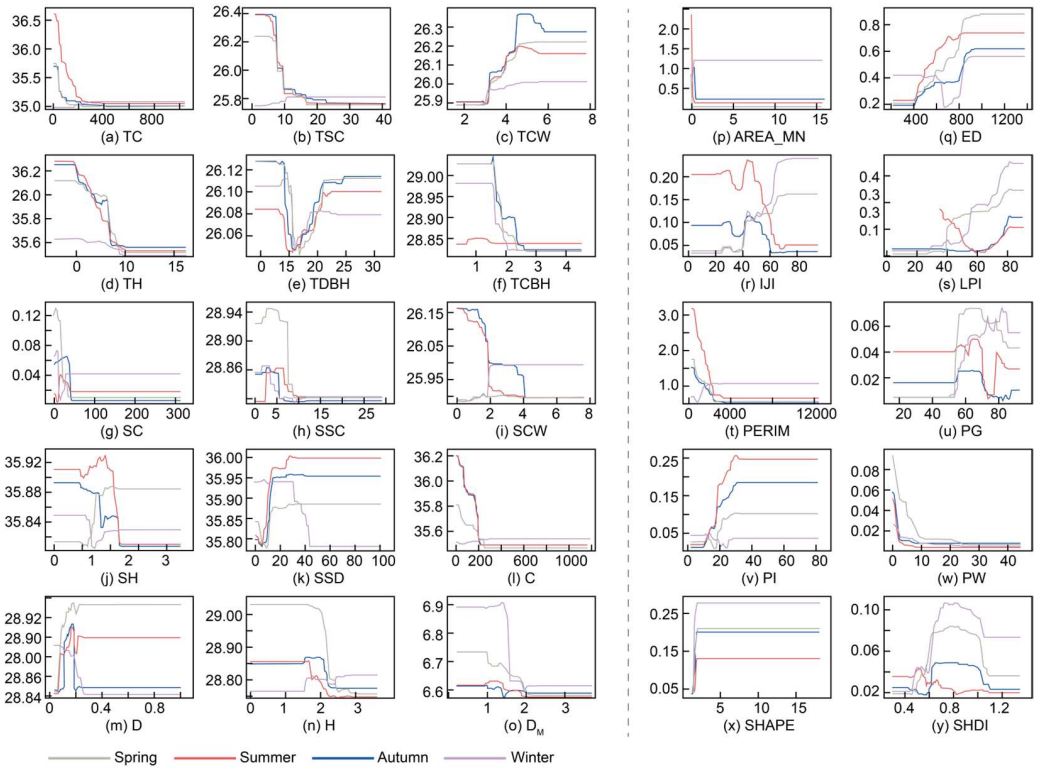

Figure 9. Partial dependence plot of the driving factors' impact on LST.

The marginal effects of the LM on LST exhibit seasonal variations. Throughout the year, SHAPE shows a significant positive contribution to LST, while PW overall exhibits a decreasing trend in its contribution, with the maximum cooling effect in spring (0.09 °C) and the minimum in winter (0.03 °C). During spring, summer, and autumn, PI and ED demonstrate a fluctuating upward trend in their control over park LST, with the strongest influence observed during summer, whereas PERIM and AREA_MN exhibit the opposite trend. In summer, as SHDI increases, LST shows a declining pattern, and when SHDI reaches 1.05, its impact on LST remains relatively stable. LPI exhibits a decreasing and then increasing trend during summer, with a turning point at LPI 60. In other seasons, as LPI increases within the range of 30–90, LST rises. In summer, PG's contribution to LST shows an opposite pattern compared to other seasons, characterized by a decrease followed by a rebound.

4. Discussion

4.1. Seasonal Variations in LST in Parks

Most of the related studies in Zhengzhou City have focused on correlating changes in LST with urbanization level or gradients [39–41], investigating the drivers influencing LST including different land cover types, the LM, human activities, and urban habitat quality [42–44], or examining the interannual thermal effect change trends and predictions [40,45,46]. However, there is relatively limited research specifically analyzing the seasonal variations of thermal effects in parks and green spaces.

Our results indicate that the average LST in parks in Zhengzhou City is lower by 0.65–2.84 °C compared to the urban areas in all seasons, with the most significant heat mitigation effect observed in autumn, reaching up to 5.15 °C. This cooling effect surpasses the temperature reduction ranges observed in ten large parks in Beijing (0.11–3.22 °C) [47], parks in Nanjing (0.6 °C), and the average temperature reduction in urban parks from 16 studies worldwide (0.94 °C) [48], while it is lower than the temperature reduction observed in 21 parks in Ethiopia (3.93 °C) [49] and the average temperature reduction in 30 parks in Beijing (3.55 °C) [50]. The maximum temperature reduction in our study occurred in autumn, reaching 5.15 °C, which is less than the maximum temperature reduction observed in a 0.24–hectare urban park in the capital of Portugal (9 °C) [51] and in 92 parks in Nagoya, Japan (7.26 °C) [52].

The seasonal analysis of urban park LST revealed that parks in Zhengzhou exhibit the strongest alleviation effect on urban heat during autumn, followed by summer and spring, while winter shows an increase in LST, which differs from similar research results. Studies conducted in Japan and Changchun also suggest a more pronounced cooling effect of park green spaces in summer [53,54]. Firstly, our findings align with previous research, indicating that urban park green spaces are important urban landscapes for regulating the thermal environment [14,55,56]. However, differences in average cooling intensity, maximum cooling effect, and seasonal variations among different cities are greatly influenced by research measurement methods and time. A study on the spatiotemporal variations of UHI intensity reveals that cities with similar climatic conditions may exhibit notable disparities in UHI intensity. The scale of the population primarily influences the generation of anthropogenic heat, although additional structural and climatic elements also influence UHI variability [57]. Furthermore, the correlation between urban parks and surface thermal conditions varies based on local climates, showcasing diverse ecological traits across different climate regions [58]. In warmer climates, urban park green spaces exert a more pronounced cooling influence on LST [51,59]. This seasonal difference is associated with solar radiation, air humidity, and rainfall [60], which indirectly influence vegetation and further impact LST through feedback mechanisms. Multiple studies have validated the notable correlation between park cooling effects and the geographical, climatic, and topographic characteristics of surveyed parks [48,61]. The seasonal variation in solar altitude leads to higher solar radiation during spring and summer, while the radiation is lowest in winter. Unlike other seasons, the combined effects of heat sources and emissions in winter

result in a weaker overall mitigation effect on LST throughout the year [62]. Additionally, the presence of leaf litter in winter significantly increases radiation reflectance [63,64]. Prior research has mainly focused on analyzing LST in individual large parks, and limitations in satellite pixel resolution may omit or misidentify numerous small park green spaces as impervious urban surfaces [65]. However, it is crucial not to overlook small-scale parks, as urban park green spaces are highly dispersed, heterogeneous, and dynamic. Previous studies have underscored the considerable cooling benefits that small parks can provide to their surrounding areas [66,67]. Zhengzhou has 32 parks with an area less than 2 hectares, exhibiting an average cooling magnitude of 0.30 °C.

4.2. Impact Factors Driving LST

As urban LST decreases, the certainty surrounding the driving factors of vegetation indices on urban LST diminishes, and the overall driving process becomes more complex. The spatiotemporal variations and mechanisms influencing LST also become more intricate, consistent with Peng et al.'s findings [24]. Our findings suggest that different VCI values exert a notable negative impact on LST, and overall, trees exhibit a stronger cooling effect on LST compared to shrubs. This aligns with prior studies, highlighting the significant influence of tree–shrub configuration and composition on surface thermal effects in urban parks, as confirmed in Cao et al.'s study on parks in Nagoya, Japan [68]. The study reveals that vegetation characteristics contribute significantly to LST during autumn, and the correlation with LST is stronger during spring and autumn. The number of trees and shrubs is closely related to the differences in LST in urban parks, with areas having a higher vegetation quantity generally exhibiting lower LST [69].

The differences in vegetation types are also an important factor contributing to variations in regional LST research results. Refs. [70,71] found that coniferous trees, due to their lower leaf density compared to broad-leaved trees, allow more solar radiation to penetrate through the canopy, leading to a stronger cooling effect in areas with coniferous vegetation compared to those with broad-leaved vegetation. Additionally, variations in vegetation phenology among species, influenced by the climatic zone of the study area, also contribute to the seasonal fluctuations of LST [72]. Furthermore, factors such as artificial maintenance, irrigation, and rainfall can have a significant impact on the extent and range of vegetation-induced LST reduction [73].

The LM of urban parks exhibits a greater driving effect on LST in most seasons compared to the VCI. Numerous studies have shown a strong correlation between changes in LST within urban areas and landscape composition and pattern [74,75]. Vegetation and water bodies effectively lower LST, aligning with previous research, whereas non-permeable surfaces have the opposite effect [39,41,46].

Specifically, vegetation and water bodies exhibit a notable cooling effect on LST during summer and autumn, although this effect diminishes during winter. Additionally, water bodies have a more substantial impact on LST compared to vegetation [58,60,76–78]. During winter, with reduced solar radiation, the UHI effect is primarily caused by human activities and pollution, resulting in a lesser influence of land cover types [79].

AREA_MN, PERIM, and LPI exhibit stronger negative influence on LST across all seasons. AREA_MN and LPI, as measures of park patch fragmentation [80], suggest that heightened landscape fragmentation worsens surface thermal conditions. [39] also found a significant negative effect of AREA_MN on LST in spring in Zhengzhou, and the influence of park perimeter and landscape fragmentation on LST has been confirmed in studies conducted in many other cities [58,81–83]. Research findings suggest that a rise in shape index correlates with a notable increase in LST, aligning with similar conclusions drawn from studies conducted in Japan [68]. IJI, SHDI, and ED have a clear positive impact on LST in all seasons, except for summer, when the impact is reversed. This suggests that denser and more evenly distributed patches within the park, along with a higher degree of fragmentation at the patch boundaries, result in higher LST, which is also corroborated by other studies [19,84,85].

4.3. Implications for Future Urban Planning and Management

Based on the findings of this study regarding UHI effect, various recommendations and measures can be proposed for different parks:

In community parks, increasing species richness may help achieve the cooling threshold. This could potentially be done by transplanting or preserving large trees on site to enhance TDBH. Care and reduced pruning of shrubs might also be implemented to increase the SH and alleviate the surface thermal environment. Additionally, since this type of park usually has a low proportion of water bodies, incorporating small-scale water reservoirs or introducing flowing water could enhance the proportion of water bodies. Due to PERIM's high contribution, merging scattered land parcels and increasing the park's perimeter is likely to be beneficial.

For theme parks, the relative importance of AREA_MN appears to be significantly stronger than other indicators, so it may be advisable to appropriately increase the proportion of individual patches. This could potentially be achieved by enlarging the area of green spaces or specific architectural features to enhance the proportion of dominant patches in the landscape. Regarding plant selection, various types of trees and shrubs might be planted to enhance species diversity. Attention should be given to plant maintenance practices that promote larger SCW and TH. Selecting tree species that naturally grow taller or pruning existing trees to increase branch height could enhance the cooling effects of urban parks.

In smaller parks, focusing on enhancing the overall coherence of the landscape and minimizing patch fragmentation is advisable. Increasing the proportion of green spaces appropriately might help achieve the maximum cooling threshold. In terms of vegetation, selecting plant species with larger canopy sizes is recommended to maximize the cooling effect on LST. When selecting trees for medium parks, it is generally recommended to choose species with a height greater than 5 m and a branch height ranging from 2 to 2.5 m. Increasing the diversity of shrub species and ensuring a minimum of three shrub species per one hundred square meters can be important. In terms of landscape layout, efforts should be made to reduce patch fragmentation. Increasing the proportion of water bodies through the addition of features such as fountains, natural wetlands, or small depressions acting as water reservoirs may help lower LST in medium parks while enhancing the overall park landscape.

In dry parks, it is recommended to increase the density of trees to at least twenty trees per one hundred square meters. Control measures should be implemented to limit SSC to less than three per one hundred square meters, while still meeting the threshold for increasing LST. In terms of landscape pattern, a water body proportion of approximately 10% might achieve maximum cooling intensity within the smallest area. Additionally, enhancing the diversity of landscape patches and striving for an even distribution of various patch types could help reduce the dominance of the largest patch and contribute to mitigating LST.

4.4. Limitations and Suggestions

Firstly, this study utilized remote sensing data to quantitatively analyze seasonal LST, recognizing that the thermal environment of the land surface is influenced by various atmospheric physical factors to a certain extent. Therefore, future research should focus on supplementing remote sensing thermal data with field meteorological survey data to enhance research accuracy by incorporating multiple data sources. Secondly, in the investigation of the VCI, due to constraints in time and cost, although this study defined 805 sample plots for park sampling, some data gaps exist compared to a comprehensive census, meaning the sampling may not be fully comprehensive. Moreover, ground cover plants were not considered in this study due to the complexity of mixed planting in urban parks, which makes it difficult to survey these species accurately. Thirdly, beyond the intrinsic characteristics of green spaces affecting park LST, the surrounding built environment also plays a significant role. Factors such as location and adjacent building facades contribute

to this influence. Future research would benefit from integrating these factors into the research framework for a more comprehensive analysis of land surface temperature in urban park green spaces. Additionally, the external environment surrounding urban parks, such as topography [86], nearby landforms [87], and the built environment [88], may also impact the parks' cooling effects. These external factors can potentially influence or even modulate the effectiveness of the cooling provided by urban green spaces. However, this study did not consider the role of the external environment in shaping the parks' thermal regulation. This represents a limitation of our current analysis. Future research should incorporate these external influences to better understand how urban parks' cooling effects are affected by their broader surroundings.

5. Conclusions

This study integrates remote sensing and vegetation survey data to examine how the VCI and LM affect LST across various seasons and park types in Zhengzhou City. The key findings are: (1) Seasonal variations exist in the cooling effect of green spaces in Zhengzhou City. During autumn, summer, and winter, the average LST decreases by 2.89 °C, 1.41 °C, and 0.65 °C, respectively, compared to urban areas. However, in winter, it increases by 1.92 °C. (2) Notable LST differences among various park types are evident in spring, summer, and autumn. However, in winter, distinctions primarily occur within park areas. Community parks, comprehensive parks, large parks, and water-themed parks display more distinct temperature variations on the land surface. (3) The LM contributes more to LST than the VCI in spring, summer, and winter, whereas in autumn, the opposite is observed. (4) For all parks in the study area, parks with longer perimeters, larger patch areas, more dispersed distribution, higher plant community richness, taller vegetation, and larger crown width demonstrate better regulatory capabilities in mitigating the deterioration of urban thermal environments. The innovation of this study lies in investigating the differences in LST drivers across various types of urban parks, an area that has not been fully explored in previous research, especially in inland cities like Zhengzhou. By utilizing machine learning regression and partial dependence analysis, the study assesses the contributions of different drivers in various park types and develops targeted strategies to mitigate UHI effects in urban parks, ultimately enhancing the comfort and sustainability of urban living environments.

Author Contributions: Conceptualization, Y.F. and K.Z.; methodology, S.G., Y.Z. and Y.F.; software, Y.F.; validation, A.L., K.W., N.D. and R.H.; formal analysis, Y.F. and K.Z.; investigation, P.S., S.G. and N.G.; resources, P.S. and X.X.; data curation, H.Y.W.; writing—original draft preparation, K.Z. and Y.F.; writing—review and editing, Y.F. and S.G.; visualization, Y.F.; supervision, R.H.; project administration, X.T. and L.F.; funding acquisition, S.G., B.W. and P.S. All authors have read and agreed to the published version of the manuscript.

Funding: This research was funded by the National Natural Science Foundation of China, grant number 32460421 and 52208056; the Key Technology R&D Program of Henan Province, grant number 232102320190 and 242102320320; the Special Fund for Young Talents in Henan Agricultural University, grant number 30500930 and 30501053; and the 2018 Henan Provincial Financial Land Re-search Project (Yu Guo Tu Zi Fa [2018] No. 125-1).

Data Availability Statement: The original contributions presented in the study are included in the article; further inquiries can be directed to the corresponding author.

Conflicts of Interest: Author Long Fan was employed by the company Henan Urban and Rural Planning and Design Research Institute Co., Ltd. The remaining authors declare that the research was conducted in the absence of any commercial or financial relationships that could be construed as a potential conflict of interest.

Appendix A

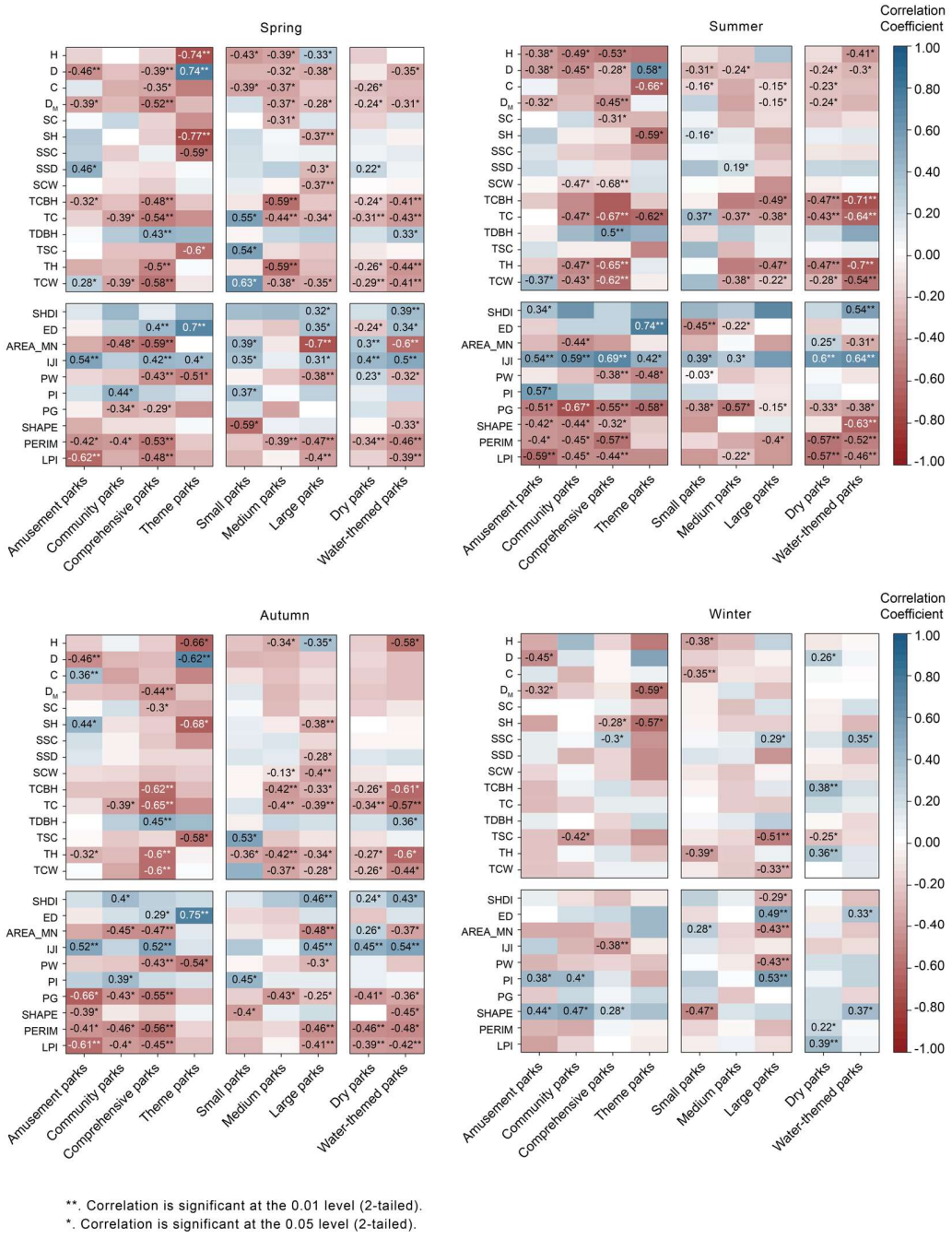

Figure A1. The correlation between each driving factor and LST in different park types and seasons.

References

1. United Nations. *68% of the World Population Projected to Live in Urban Areas by 2050, Says UN*; United Nations: New York, NY, USA, 2018.
2. Li, B.; Chen, C.; Hu, B. Governing Urbanization and the New Urbanization Plan in China. *Environ. Urban.* **2016**, *28*, 515–534. [CrossRef]
3. Ventriglio, A.; Torales, J.; Castaldelli-Maia, J.M.; Berardis, D.D.; Bhugra, D. Urbanization and Emerging Mental Health Issues. *CNS Spectr.* **2021**, *26*, 43–50. [CrossRef] [PubMed]
4. Wu, J.; Xiang, W.-N.; Zhao, J. Urban Ecology in China: Historical Developments and Future Directions. *Landsc. Urban Plan.* **2014**, *125*, 222–233. [CrossRef]
5. Liang, L.; Wang, Z.; Li, J. The Effect of Urbanization on Environmental Pollution in Rapidly Developing Urban Agglomerations. *J. Clean. Prod.* **2019**, *237*, 117649. [CrossRef]

6. Li, G.; Zhang, X.; Mirzaei, P.A.; Zhang, J.; Zhao, Z. Urban Heat Island Effect of a Typical Valley City in China: Responds to the Global Warming and Rapid Urbanization. *Sustain. Cities Soc.* **2018**, *38*, 736–745. [CrossRef]
7. Augusto, B.; Roebeling, P.; Rafael, S.; Ferreira, J.; Ascenso, A.; Bodilis, C. Short and Medium- to Long-Term Impacts of Nature-Based Solutions on Urban Heat. *Sustain. Cities Soc.* **2020**, *57*, 102122. [CrossRef]
8. Founda, D.; Santamouris, M. Synergies between Urban Heat Island and Heat Waves in Athens (Greece), during an Extremely Hot Summer (2012). *Sci. Rep.* **2017**, *7*, 10973. [CrossRef]
9. Tan, J.; Zheng, Y.; Tang, X.; Guo, C.; Li, L.; Song, G.; Zhen, X.; Yuan, D.; Kalkstein, A.J.; Li, F.; et al. The Urban Heat Island and Its Impact on Heat Waves and Human Health in Shanghai. *Int. J. Biometeorol.* **2010**, *54*, 75–84. [CrossRef]
10. Patz, J.A.; Campbell-Lendrum, D.; Holloway, T.; Foley, J.A. Impact of Regional Climate Change on Human Health. *Nature* **2005**, *438*, 310–317. [CrossRef]
11. Chow, W.T.L.; Pope, R.L.; Martin, C.A.; Brazel, A.J. Observing and Modeling the Nocturnal Park Cool Island of an Arid City: Horizontal and Vertical Impacts. *Theor. Appl. Clim.* **2011**, *103*, 197–211. [CrossRef]
12. Su, Y.; Wu, J.; Zhang, C.; Wu, X.; Li, Q.; Liu, L.; Bi, C.; Zhang, H.; Lafortezza, R.; Chen, X. Estimating the Cooling Effect Magnitude of Urban Vegetation in Different Climate Zones Using Multi-Source Remote Sensing. *Urban Clim.* **2022**, *43*, 101155. [CrossRef]
13. Qiu, G.; Li, H.; Zhang, Q.; Chen, W.; Liang, X.; Li, X. Effects of Evapotranspiration on Mitigation of Urban Temperature by Vegetation and Urban Agriculture. *J. Integr. Agric.* **2013**, *12*, 1307–1315. [CrossRef]
14. Sun, R.; Chen, L. Effects of Green Space Dynamics on Urban Heat Islands: Mitigation and Diversification. *Ecosyst. Serv.* **2017**, *23*, 38–46. [CrossRef]
15. Debbage, N.; Shepherd, J.M. The Urban Heat Island Effect and City Contiguity. *Comput. Environ. Urban Syst.* **2015**, *54*, 181–194. [CrossRef]
16. Stuhlmacher, M.; Georgescu, M.; Turner, B.L.; Hu, Y.; Goldblatt, R.; Gupta, S.; Frazier, A.E.; Kim, Y.; Balling, R.C.; Clinton, N. Are Global Cities Homogenizing? An Assessment of Urban Form and Heat Island Implications. *Cities* **2022**, *126*, 103705. [CrossRef]
17. Abdulmana, S.; Garcia-Constantino, M.; Lim, A. The Influence of Elevation, Land Cover and Vegetation Index on LST Increase in Taiwan from 2000 to 2021. *Sustainability* **2023**, *15*, 3262. [CrossRef]
18. Peng, W.; Yuan, X.; Gao, W.; Wang, R.; Chen, W. Assessment of Urban Cooling Effect Based on Downscaled Land Surface Temperature: A Case Study for Fukuoka, Japan. *Urban Clim.* **2021**, *36*, 100790. [CrossRef]
19. Xiang, Y.; Ye, Y.; Peng, C.; Teng, M.; Zhou, Z. Seasonal Variations for Combined Effects of Landscape Metrics on Land Surface Temperature (LST) and Aerosol Optical Depth (AOD). *Ecol. Indic.* **2022**, *138*, 108810. [CrossRef]
20. Gabriel, K.M.A.; Endlicher, W.R. Urban and Rural Mortality Rates during Heat Waves in Berlin and Brandenburg, Germany. *Environ. Pollut.* **2011**, *159*, 2044–2050. [CrossRef]
21. Kim, M.; Lee, K.; Cho, G.-H. Temporal and Spatial Variability of Urban Heat Island by Geographical Location: A Case Study of Ulsan, Korea. *Build. Environ.* **2017**, *126*, 471–482. [CrossRef]
22. Chapman, S.; Thatcher, M.; Salazar, A.; Watson, J.E.M.; McAlpine, C.A. The Impact of Climate Change and Urban Growth on Urban Climate and Heat Stress in a Subtropical City. *Int. J. Climatol.* **2019**, *39*, 3013–3030. [CrossRef]
23. Liu, Y.; Li, Q.; Yang, L.; Mu, K.; Zhang, M.; Liu, J. Urban Heat Island Effects of Various Urban Morphologies under Regional Climate Conditions. *Sci. Total Environ.* **2020**, *743*, 140589. [CrossRef]
24. Peng, J.; Jia, J.; Liu, Y.; Li, H.; Wu, J. Seasonal Contrast of the Dominant Factors for Spatial Distribution of Land Surface Temperature in Urban Areas. *Remote Sens. Environ.* **2018**, *215*, 255–267. [CrossRef]
25. Tran, D.X.; Pla, F.; Latorre-Carmona, P.; Myint, S.W.; Caetano, M.; Kieu, H.V. Characterizing the Relationship between Land Use Land Cover Change and Land Surface Temperature. *ISPRS J. Photogramm.* **2017**, *124*, 119–132. [CrossRef]
26. Guo, A.; Yang, J.; Xiao, X.; Xia, J.; Jin, C.; Li, X. Influences of Urban Spatial Form on Urban Heat Island Effects at the Community Level in China. *Sustain. Cities Soc.* **2020**, *53*, 101972. [CrossRef]
27. Han, D.; An, H.; Wang, F.; Xu, X.; Qiao, Z.; Wang, M.; Sui, X.; Liang, S.; Hou, X.; Cai, H.; et al. Understanding Seasonal Contributions of Urban Morphology to Thermal Environment Based on Boosted Regression Tree Approach. *Build. Environ.* **2022**, *226*, 109770. [CrossRef]
28. Özhancı, E.; Koç, A. The Effect of Different Area Uses and Topography on Surface Temperature and Climate Parameters. *Environ. Sci. Pollut. Res.* **2023**, *30*, 47038–47051. [CrossRef]
29. Saavedra, M.; Junquas, C.; Espinoza, J.-C.; Silva, Y. Impacts of Topography and Land Use Changes on the Air Surface Temperature and Precipitation over the Central Peruvian Andes. *Atmos. Res.* **2020**, *234*, 104711. [CrossRef]
30. Xin, J.; Yang, J.; Sun, D.; Han, T.; Song, C.; Shi, Z. Seasonal Differences in Land Surface Temperature under Different Land Use/Land Cover Types from the Perspective of Different Climate Zones. *Land* **2022**, *11*, 1122. [CrossRef]
31. Yuan, B.; Li, X.; Zhou, L.; Bai, T.; Hu, T.; Huang, J.; Liu, D.; Li, Y.; Guo, J. Global Distinct Variations of Surface Urban Heat Islands in Inter- and Intra-Cities Revealed by Local Climate Zones and Seamless Daily Land Surface Temperature Data. *ISPRS J. Photogramm. Remote Sens.* **2023**, *204*, 1–14. [CrossRef]
32. Peng, J.; Dan, Y.; Qiao, R.; Liu, Y.; Dong, J.; Wu, J. How to Quantify the Cooling Effect of Urban Parks? Linking Maximum and Accumulation Perspectives. *Remote Sens. Environ.* **2021**, *252*, 112135. [CrossRef]
33. Zhou, T.; Jia, W.; Yan, L.; Hong, B.; Wang, K. Urban Park's Vertical Canopy Structure and Its Varied Cooling Effect under Continuous Warming Climate. *Urban Clim.* **2024**, *53*, 101819. [CrossRef]

34. Zhang, K.; Yun, G.; Song, P.; Wang, K.; Li, A.; Du, C.; Jia, X.; Feng, Y.; Wu, M.; Qu, K.; et al. Discover the Desirable Landscape Structure of Urban Parks for Mitigating Urban Heat: A High Spatial Resolution Study Using a Forest City, Luoyang, China as a Lens. *Int. J. Environ. Res. Public Health* **2023**, *20*, 3155. [CrossRef] [PubMed]
35. Sobrino, J.A.; Juan, C. Jiménez-Muoz, J.C. Leonardo Paolini Land Surface Temperature Retrieval from LANDSAT TM 5. *Remote Sens. Environ.* **2004**, *90*, 434–440. [CrossRef]
36. Carlson, T.N.; Ripley, D.A. On the Relation between NDVI, Fractional Vegetation Cover, and Leaf Area Index. *Remote Sens. Environ.* **1997**, *62*, 241–252. [CrossRef]
37. Huang, J.; Wang, Y. Cooling Intensity of Hybrid Landscapes in a Metropolitan Area: Relative Contribution and Marginal Effect. *Sustain. Cities Soc.* **2022**, *79*, 103725. [CrossRef]
38. Li, Z.; Hu, D. Exploring the Relationship between the 2D/3D Architectural Morphology and Urban Land Surface Temperature Based on a Boosted Regression Tree: A Case Study of Beijing, China. *Sustain. Cities Soc.* **2022**, *78*, 103392. [CrossRef]
39. Du, C.; Song, P.; Wang, K.; Li, A.; Hu, Y.; Zhang, K.; Jia, X.; Feng, Y.; Wu, M.; Qu, K.; et al. Investigating the Trends and Drivers between Urbanization and the Land Surface Temperature: A Case Study of Zhengzhou, China. *Sustainability* **2022**, *14*, 13845. [CrossRef]
40. Min, M.; Zhao, H.; Miao, C. Spatio-Temporal Evolution Analysis of the Urban Heat Island: A Case Study of Zhengzhou City, China. *Sustainability* **2018**, *10*, 1992. [CrossRef]
41. Yang, H.; Xi, C.; Zhao, X.; Mao, P.; Wang, Z.; Shi, Y.; He, T.; Li, Z. Measuring the Urban Land Surface Temperature Variations Under Zhengzhou City Expansion Using Landsat-Like Data. *Remote Sens.* **2020**, *12*, 801. [CrossRef]
42. Li, B.; Shi, X.; Wang, H.; Qin, M. Analysis of the Relationship between Urban Landscape Patterns and Thermal Environment: A Case Study of Zhengzhou City, China. *Environ. Monit. Assess.* **2020**, *192*, 540. [CrossRef] [PubMed]
43. Zhao, H.; Tan, J.; Ren, Z.; Wang, Z. Spatiotemporal Characteristics of Urban Surface Temperature and Its Relationship with Landscape Metrics and Vegetation Cover in Rapid Urbanization Region. *Complexity* **2020**, *2020*, 7892362. [CrossRef]
44. Zhou, X.; Chen, H. Experimental Analysis of the Influence of Urban Morphological Indices on the Urban Thermal Environment of Zhengzhou, China. *Atmosphere* **2021**, *12*, 1058. [CrossRef]
45. Zhang, X.; Xiao, Y.; Zhu, G.; Shi, J. A Coupled CEEMD-BiLSTM Model for Regional Monthly Temperature Prediction. *Environ. Monit. Assess.* **2023**, *195*, 379. [CrossRef]
46. Zhou, S.; Liu, D.; Zhu, M.; Tang, W.; Chi, Q.; Ye, S.; Xu, S.; Cui, Y. Temporal and Spatial Variation of Land Surface Temperature and Its Driving Factors in Zhengzhou City in China from 2005 to 2020. *Remote Sens.* **2022**, *14*, 4281. [CrossRef]
47. Li, Y.; Fan, S.; Li, K.; Zhang, Y.; Kong, L.; Xie, Y.; Dong, L. Large Urban Parks Summertime Cool and Wet Island Intensity and Its Influencing Factors in Beijing, China. *Urban For. Urban Green.* **2021**, *65*, 127375. [CrossRef]
48. Bowler, D.E.; Buyung-Ali, L.; Knight, T.M.; Pullin, A.S. Urban Greening to Cool Towns and Cities: A Systematic Review of the Empirical Evidence. *Landsc. Urban Plan.* **2010**, *97*, 147–155. [CrossRef]
49. Feyisa, G.L.; Dons, K.; Meilby, H. Efficiency of Parks in Mitigating Urban Heat Island Effect: An Example from Addis Ababa. *Landsc. Urban Plan.* **2014**, *123*, 87–95. [CrossRef]
50. Lin, W.; Yu, T.; Chang, X.; Wu, W.; Zhang, Y. Calculating Cooling Extents of Green Parks Using Remote Sensing: Method and Test. *Landsc. Urban Plan.* **2015**, *134*, 66–75. [CrossRef]
51. Oliveira, S.; Andrade, H.; Vaz, T. The Cooling Effect of Green Spaces as a Contribution to the Mitigation of Urban Heat: A Case Study in Lisbon. *Build. Environ.* **2011**, *46*, 2186–2194. [CrossRef]
52. Onishi, A.; Xin, C.; Ito, T.; Shi, F.; Imura, H. Evaluating the Potential for Urban Heat-Island Mitigation by Greening Parking Lots. *Urban For. Urban Green.* **2010**, *9*, 323–332. [CrossRef]
53. Hamada, S.; Ohta, T. Seasonal Variations in the Cooling Effect of Urban Green Areas on Surrounding Urban Areas. *Urban For. Urban Green.* **2010**, *9*, 15–24. [CrossRef]
54. Yang, C.; He, X.; Wang, R.; Yan, F.; Yu, L.; Bu, K.; Yang, J.; Chang, L.; Zhang, S. The Effect of Urban Green Spaces on the Urban Thermal Environment and Its Seasonal Variations. *Forests* **2017**, *8*, 153. [CrossRef]
55. Ca, V.T.; Asaeda, T.; Abu, E.M. Reductions in air conditioning energy caused by a nearby park. *Energy Build.* **1998**, *29*, 83–92. [CrossRef]
56. Yao, L.; Li, T.; Xu, M.; Xu, Y. How the Landscape Features of Urban Green Space Impact Seasonal Land Surface Temperatures at a City-Block-Scale: An Urban Heat Island Study in Beijing, China. *Urban For. Urban Green.* **2020**, *52*, 126704. [CrossRef]
57. Nwakaire, C.M.; Onn, C.C.; Yap, S.P.; Yuen, C.W.; Onodagu, P.D. Urban Heat Island Studies with Emphasis on Urban Pavements: A Review. *Sustain. Cities Soc.* **2020**, *63*, 102476. [CrossRef]
58. Yang, Q.; Huang, X.; Li, J. Assessing the Relationship between Surface Urban Heat Islands and Landscape Patterns across Climatic Zones in China. *Sci. Rep.* **2017**, *7*, 9337. [CrossRef]
59. Lin, B.-S.; Lin, Y.-J. Cooling Effect of Shade Trees with Different Characteristics in a Subtropical Urban Park. *Hortscience* **2010**, *45*, 83–86. [CrossRef]
60. Cao, S.; Sanchez-Azofeifa, A. Modeling Seasonal Surface Temperature Variations in Secondary Tropical Dry Forests. *Int. J. Appl. Earth Obs. Geoinf.* **2017**, *62*, 122–134. [CrossRef]
61. Aram, F.; García, E.H.; Solgi, E.; Mansournia, S. Urban Green Space Cooling Effect in Cities. *Heliyon* **2019**, *5*, e01339. [CrossRef]
62. Wu, W.; Li, L.; Li, C. Seasonal Variation in the Effects of Urban Environmental Factors on Land Surface Temperature in a Winter City. *J. Clean. Prod.* **2021**, *299*, 126897. [CrossRef]

63. Chen, L.; Wang, X.; Cai, X.; Yang, C.; Lu, X. Seasonal Variations of Daytime Land Surface Temperature and Their Underlying Drivers over Wuhan, China. *Remote Sens.* **2021**, *13*, 323. [CrossRef]
64. Zhang, W.; Jiang, J.; Zhu, Y. Change in Urban Wetlands and Their Cold Island Effects in Response to Rapid Urbanization. *Chin. Geogr. Sci.* **2015**, *25*, 462–471. [CrossRef]
65. Haase, D.; Jänicke, C.; Wellmann, T. Front and Back Yard Green Analysis with Subpixel Vegetation Fractions from Earth Observation Data in a City. *Landsc. Urban. Plan.* **2019**, *182*, 44–54. [CrossRef]
66. Park, J.; Kim, J.-H.; Lee, D.K.; Park, C.Y.; Jeong, S.G. The Influence of Small Green Space Type and Structure at the Street Level on Urban Heat Island Mitigation. *Urban. For. Urban Green.* **2017**, *21*, 203–212. [CrossRef]
67. Wu, C.; Li, J.; Wang, C.; Song, C.; Finka, M. Estimating the Cooling Effect of Pocket Green Space in High Density Urban Areas in Shanghai, China. *Front. Environ. Sci.* **2021**, *9*, 657969. [CrossRef]
68. Cao, X.; Onishi, A.; Chen, J.; Imura, H. Quantifying the Cool Island Intensity of Urban Parks Using ASTER and IKONOS Data. *Landsc. Urban Plan.* **2010**, *96*, 224–231. [CrossRef]
69. Jenerette, G.D.; Harlan, S.L.; Brazel, A.; Jones, N.; Larsen, L.; Stefanov, W.L. Regional Relationships between Surface Temperature, Vegetation, and Human Settlement in a Rapidly Urbanizing Ecosystem. *Landsc. Ecol.* **2007**, *22*, 353–365. [CrossRef]
70. Eyster, H.N.; Beckage, B. Conifers May Ameliorate Urban Heat Waves Better Than Broadleaf Trees: Evidence from Vancouver, Canada. *Atmosphere* **2022**, *13*, 830. [CrossRef]
71. Li, Z.; Zheng, H. Cooling and Humidification Effects of Coniferous and Broad-Leaved Plant Communities in Urban Park. *Build. Environ.* **2023**, *245*, 110892. [CrossRef]
72. Yuan, F.; Bauer, M.E. Comparison of Impervious Surface Area and Normalized Difference Vegetation Index as Indicators of Surface Urban Heat Island Effects in Landsat Imagery. *Remote Sens. Environ.* **2007**, *106*, 375–386. [CrossRef]
73. Yu, Z.; Xu, S.; Zhang, Y.; Jorgensen, G.; Vejre, H. Strong Contributions of Local Background Climate to the Cooling Effect of Urban Green Vegetation. *Sci. Rep.* **2018**, *8*, 6798. [CrossRef] [PubMed]
74. Huang, G.; Cadenasso, M.L. People, Landscape, and Urban Heat Island: Dynamics among Neighborhood Social Conditions, Land Cover and Surface Temperatures. *Landsc. Ecol.* **2016**, *31*, 2507–2515. [CrossRef]
75. Asgarian, A.; Amiri, B.J.; Sakieh, Y. Assessing the Effect of Green Cover Spatial Patterns on Urban Land Surface Temperature Using Landscape Metrics Approach. *Urban Ecosyst.* **2015**, *18*, 209–222. [CrossRef]
76. Xue, Y.; Lu, H.; Guan, Y.; Tian, P.; Yao, T. Impact of Thermal Condition on Vegetation Feedback under Greening Trend of China. *Sci. Total Environ.* **2021**, *785*, 147380. [CrossRef]
77. Chen, J.; Jin, S.; Du, P. Roles of Horizontal and Vertical Tree Canopy Structure in Mitigating Daytime and Nighttime Urban Heat Island Effects. *Int. J. Appl. Earth Obs. Geoinf.* **2020**, *89*, 102060. [CrossRef]
78. Klok, L.; Zwart, S.; Verhagen, H.; Mauri, E. The Surface Heat Island of Rotterdam and Its Relationship with Urban Surface Characteristics. *Resour. Conserv. Recycl.* **2012**, *64*, 23–29. [CrossRef]
79. Yang, C.; Yan, F.; Lei, X.; Ding, X.; Zheng, Y.; Liu, L.; Zhang, S. Investigating Seasonal Effects of Dominant Driving Factors on Urban Land Surface Temperature in a Snow-Climate City in China. *Remote Sens.* **2020**, *12*, 3006. [CrossRef]
80. Liu, C.-F.; Li, J.-Z.; Li, X.-M.; He, X.-Y.; Chen, W. Selection of landscape metrics for urban forest based on simulated landscapes. *Ying Yong Sheng Tai Xue Bao* **2009**, *20*, 1125–1131.
81. Xie, M.; Wang, Y.; Chang, Q.; Fu, M.; Ye, M. Assessment of Landscape Patterns Affecting Land Surface Temperature in Different Biophysical Gradients in Shenzhen, China. *Urban Ecosyst.* **2013**, *16*, 871–886. [CrossRef]
82. Masoudi, M.; Tan, P.Y. Multi-Year Comparison of the Effects of Spatial Pattern of Urban Green Spaces on Urban Land Surface Temperature. *Landsc. Urban Plan.* **2019**, *184*, 44–58. [CrossRef]
83. Yin, J.; Wu, X.; Shen, M.; Zhang, X.; Zhu, C.; Xiang, H.; Shi, C.; Guo, Z.; Li, C. Impact of Urban Greenspace Spatial Pattern on Land Surface Temperature: A Case Study in Beijing Metropolitan Area, China. *Landsc. Ecol.* **2019**, *34*, 2949–2961. [CrossRef]
84. Li, X.; Zhou, W.; Ouyang, Z.; Xu, W.; Zheng, H. Spatial Pattern of Greenspace Affects Land Surface Temperature: Evidence from the Heavily Urbanized Beijing Metropolitan Area, China. *Landsc. Ecol.* **2012**, *27*, 887–898. [CrossRef]
85. Zhao, H.; Zhang, H.; Miao, C.; Ye, X.; Min, M. Linking Heat Source-Sink Landscape Patterns with Analysis of Urban Heat Islands: Study on the Fast-Growing Zhengzhou City in Central China. *Remote Sens.* **2018**, *10*, 1268. [CrossRef]
86. Zheng, Z.; Lin, X.; Chen, L.; Yan, C.; Sun, T. Effects of Urbanization and Topography on Thermal Comfort during a Heat Wave Event: A Case Study of Fuzhou, China. *Sustain. Cities Soc.* **2024**, *102*, 105233. [CrossRef]
87. Song, B.; Park, K. Mountain Valley Cold Air Flow Interactions with Urban Morphology: A Case Study of the Urban Area of Changwon, South Korea. *Landsc. Urban Plan.* **2023**, *233*, 104703. [CrossRef]
88. Badaro-Saliba, N.; Adjizian-Gerard, J.; Zaarour, R.; Najjar, G. LCZ Scheme for Assessing Urban Heat Island Intensity in a Complex Urban Area (Beirut, Lebanon). *Urban Clim.* **2021**, *37*, 100846. [CrossRef]